

Formation Control of Wheeled Robots with Vision-Based Position Measurement

Hasan Poonawala, Aykut C Satici, Nicholas Gans and Mark W Spong

Abstract—Many applications require multiple mobile robots to move with a common velocity and at fixed relative distances. We present a time-invariant, state-feedback control law and a novel vision-based pose reconstruction system that allows one differential drive robot to follow another at a constant relative distance. The control law does not require measurement or estimation of the leader robot velocity and has tunable parameters that allows one to prioritize the error bounds of the desired states. The proposed pose reconstruction algorithm is computationally inexpensive and reliable. We present experimental results on two iRobot Create robots showing the performance of the controller and vision algorithm.

I. INTRODUCTION

Multi-robot systems present a more robust and cheaper solution to certain tasks that are better performed using several low-cost robots rather than single, complex ones. A multi-robot system may be required to travel over large distances in order to reach a site related to a mission or task. While traversing the distances, it may be desirable for the robots to move in a rigid formation with fixed inter-robot distances. This gives rise to the formation control problem. Further, it is often desired that the control of these distances be done in a decentralized manner, rather than through a common supervisor or command center. Such control solutions can be applied to military maneuvers or automated highways.

Many approaches to formation control have been presented. The methods of formation control commonly employed can be classified into leader-follower methods [1], [2], behavior-based control [3], [4], variable structure control techniques [5], and consensus based methods [6], [7]. The behavior-based control methods provide the robots with actions in reaction to sensor data. The local interactions occurring throughout the team ultimately result in a formation emerging and being maintained. The behavior is often encoded using potential functions. The leader-follower methods use techniques such as input-output partial feedback linearization of the dynamics of the relative pose between two robots [2]. Another leader-follower method makes use of potential functions and virtual leaders [1]. The consensus

based methods take into account the effect of the information flow between agents on the stability and performance of formation control while designing the control law.

Visual servo control involves using vision sensors to provide feedback control. The leader-follower based formation control problem incorporating visual feedback has also received some attention [8], [9], [10], [11], [12]. The various methods of visual servoing are often categorized into two groups, Position Based Visual Servoing (PBVS) and Image Based Visual Servoing (IBVS) [13]. Both methods seek to drive the camera to a goal pose with respect to some target. In the PBVS method, the control is based on the 3D pose information reconstructed from the image. In the IBVS method, the controlled states are image features of the target.

The earliest pose reconstruction methods used knowledge of the target geometry to obtain the pose of the target. In [14], four or more non-coplanar points on the target are required. The algorithm can then compute the pose of the target from a single image. In [15], four or more coplanar points on a target can be used to determine the pose from a single image, except for certain critical configurations of the points and camera. The method involves solution of the singular value decomposition of a matrix at least once for five or more points, and twice for four points. Essential Matrix [16] and Euclidean homography [17] methods were developed, which do not require a known geometry of points on the target, however they can compute the pose of the camera (at which an image is taken) only with respect to the pose in a reference image. The relative distances are obtained up to an unknown scale factor. Knowledge of the depth of the target is required in at least one reference image in order to calculate the scale factor. The work in [12] incorporates a known length between two of points on the target into a homography-based reconstruction. This enables visual servoing of the camera to an arbitrary pose with respect to the target. The work in [18] uses a pink ball to estimate relative position between two robots, however the relative pose cannot be estimated. Another approach to pose estimation is to design nonlinear observers [19], [20]. The approaches used in leader-follower methods often require measurement of the velocity of the leader robot. Some papers address this by using estimation methods [21], [22] or nonlinear observers [23].

The work in this paper has two major contributions.

- 1) A feedback control that requires only relative pose information is proposed. The controller leads to uniform ultimate boundedness of the errors. In particular, for straight line motion of the leader robot, the bound on all coordinates can be arbitrarily decreased by increasing

H. Poonawala, A. C. Satici, and N. Gans are with the Department of Electrical Engineering, University of Texas at Dallas, Dallas, TX, USA hasanp@utdallas.edu, acsatici@utdallas.edu, ngans@utdallas.edu

Mark W Spong is the Dean of the Erik Jonsson School of Engineering and Computer Science, University of Texas at Dallas, 800 W Campbell Rd, Richardson, Texas, USA mspong@utdallas.edu

This research was partially supported by the National Science Foundation Grants ECCS 07-25433 and CMMI-0856368, by the University of Texas STARS program, and by the University of Texas at Dallas.

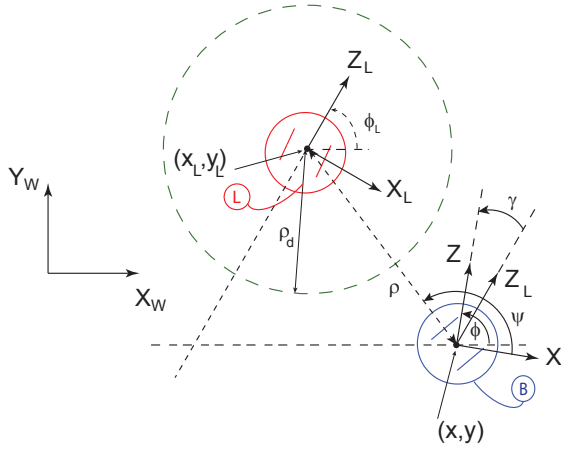


Fig. 1. WMRs in inertial and relative coordinates

the controller gains. For a general motion, only the bound on the relative distance error can be decreased arbitrarily, while the rest of the errors are ultimately bounded and this bound can be analytically characterized. Moreover, the controller possesses tunable gains which allows one to prioritize the convergence of the relative polar angle over the relative orientation or vice versa. We show in Appendix I how to find the steady state errors in the polar angle and orientation given a set of gains and the curvature of leader path. This knowledge can be used to accomplish obstacle avoidance by appropriately changing the desired polar angle.

- 2) A novel pose reconstruction method is presented, which provides reliable measurements of the state. The method exploits restricted motions of the robots, the and a known fiducial geometry. The work is similar to [15], except that the restriction to planar motions renders computations such as singular value decompositions unnecessary. A unique fiducial is used, which leads to simple and reliable extraction of feature points.

II. BACKGROUND

A. Differential-drive Wheeled Mobile Robot

Differential drive wheeled mobile robots (WMR) are popular for their low cost and simplicity, and we base our work on implementation on such robots. This type of WMR consists of a body resting on two coaxial wheels. A third castor wheel is added for support. In an inertial world reference frame, the configuration of a WMR is given by the position of the center between its two wheels (x, y) and the angle ϕ of its heading direction. The heading direction is the line perpendicular to the axes of wheel rotations, and is positive in the direction of forward motion (See Fig. 1). The kinematic equations of motion of a WMR are

$$\begin{bmatrix} \dot{x} \\ \dot{y} \\ \dot{\phi} \end{bmatrix} = \begin{bmatrix} \cos \phi & 0 \\ \sin \phi & 0 \\ 0 & 1 \end{bmatrix} \begin{bmatrix} v \\ \omega \end{bmatrix} \quad (1)$$

where v and ω are the forward speed and angular velocity of the WMR. Assume robot L with configuration (x_L, y_L, ϕ_L) has a Cartesian frame attached to it (Fig. 1). The z -axis coincides with the robot's heading direction, the y -axis (not shown in Fig. 1) is normal to the ground plane oriented downwards, and the x -axis is chosen to result in a right-handed Cartesian frame. This convention for the robot frame axes is chosen to match the convention used in labeling camera axes, since the camera optical axis and robot heading direction are assumed to be parallel in this work.

B. Relative kinematics between two WMR

Let the configurations of the leader and follower robots in the world frame be (x_L, y_L, ϕ_L) and (x, y, ϕ) respectively. In the frame of the follower, the polar coordinates of the leader are given by (ρ, ψ) . The angle that the z -axis of the leader frame makes with the z -axis of the follower is given by γ (see Fig. 1). The relative coordinates of the leader in the frame of the follower robot are then

$$\begin{bmatrix} q_1 \\ q_2 \\ q_3 \end{bmatrix} = \begin{bmatrix} ((x_L - x)^2 + (y_L - y)^2)^{\frac{1}{2}} \\ \arctan\left(\frac{y_L - y}{x_L - x}\right) - \phi \\ \phi_L - \phi \end{bmatrix} \quad (2)$$

Using (1) and differentiating (2) results in

$$\begin{bmatrix} \dot{q}_1 \\ \dot{q}_2 \\ \dot{q}_3 \end{bmatrix} = \begin{bmatrix} -c_2 & 0 \\ \frac{s_2}{q_1} & -1 \\ 0 & -1 \end{bmatrix} \begin{bmatrix} v \\ \omega \end{bmatrix} + \begin{bmatrix} c_{32} & 0 \\ \frac{s_{32}}{q_1} & 0 \\ 0 & 1 \end{bmatrix} \begin{bmatrix} v_L \\ \omega_L \end{bmatrix} \quad (3)$$

where $c_i = \cos q_i$, $s_i = \sin q_i$ and $c_{ij} = \cos(q_i - q_j)$, $s_{ij} = \sin(q_i - q_j)$. While v_L and ω_L are translational and angular velocities of the leader WMR, v and ω are translational and angular velocities of the follower WMR, respectively.

C. Camera Model

We assume the pinhole camera model for relating the image coordinates and the world coordinates of a feature point. The camera frame coincides with the robot frame. The image coordinates of a feature point $m = (m_x, m_y)$ are obtained from its 3D coordinates in the camera frame $\bar{m} = (\bar{m}_x, \bar{m}_y, \bar{m}_z)$ under perspective projection

$$m_x = f \frac{\bar{m}_x}{\bar{m}_z}, \quad m_y = f \frac{\bar{m}_y}{\bar{m}_z}$$

where f is the focal length of the camera.

III. CONTROL DESIGN

The control goal is to regulate the relative position between the follower and the leader WMRs, moving with bounded positive translational and angular velocity $(v_L, \omega_L) \in \mathbb{R}_+ \times \mathbb{R}$. This amounts to keeping (q_1, q_2) at a desired value (q_{1d}, q_{2d}) , cf. Fig. 1. Notice that this puts no restrictions on the orientation of the follower with respect to the leader. Furthermore, the nonholonomic nature of the system makes it impossible to control all three states continuously. At best, one can hope to control a combination of these three. In this work, we will be controlling q_1 and $\alpha q_2 + \beta q_3$ for some $\alpha, \beta \in \mathbb{R}$. One of the important contributions of this work is that, we can prioritize the control of q_2 over q_3 , or vice versa.

Since the pose measurements are made through a vision-based algorithm, differentiation of these inherently noisy measurements is problematic. Therefore, we will be using only relative position feedback to achieve stability. In particular, when the leader is moving in a straight line, all of the error states are uniformly ultimately bounded in the vicinity of the origin and this bound may be made arbitrarily small by increasing the controller gains. When the leader is moving with nonzero angular velocity, we again claim ultimate boundedness of the error states with the ability to make the bound on \tilde{q}_1 arbitrarily small.

Let $\tilde{q} = (\tilde{q}_1, \tilde{q}_2, \tilde{q}_3) \triangleq (q_1 - q_{1d}, q_2 - q_{2d}, q_3) \in D = \{q \in \mathbb{R}_+ \times \mathbb{R}^2 : |q_i| < \frac{\pi}{2}, i = 2, 3, |q_{1d}| > 0 \text{ and } |q_{2d}| < \frac{\pi}{2}\}$, where q_{1d} and q_{2d} are the desired values of q_1 and q_2 . The desired value q_{3d} of q_3 is assumed to be zero. Define,

$$\Lambda_1 = \left(-p_{11}c_2 + p_{22}\frac{s_2^2}{q_1^2 c_2} \right), \quad \Lambda_2 = \frac{p_{22}}{q_1^2} \left(\frac{s_2}{c_2} + s_2 \right) \quad (4a)$$

$$\Theta_1 = \left(p_{11}c_2 + p_{22}\frac{t_2 s_{32}}{q_1^2} \right) \quad (4b)$$

$$\Theta_2 = \frac{p_{22}}{q_1} (t_2 c_{32} + s_{32}) = \frac{p_{22}}{q_1} \frac{\sin q_3}{\cos q_2} \quad (4c)$$

$$\Theta_3 = \frac{p_{22}}{q_1^2} \left(\frac{s_{32}}{c_2^2} - t_2 c_{32} \right) \quad (4d)$$

Theorem III.1. *The following control law, accompanied by the conditions on the positive constants p_{ii} , given in Appendix I, ensures ultimate boundedness of the states along with the properties discussed in the previous two paragraphs.*

$$v = -k_1 (\Lambda_1 \tilde{q}_1 + \Lambda_2 \tilde{q}_1 \tilde{q}_2) \quad (5a)$$

$$\omega = k_2 \left(p_{22} \frac{t_2}{q_1} \tilde{q}_1 + p_{22} \tilde{q}_2 + p_{33} \tilde{q}_3 + \frac{p_{22}}{q_1 c_2^2} \tilde{q}_1 \tilde{q}_2 \right) \quad (5b)$$

where $t_2 := \tan q_2$, (k_1, k_2) are positive constants and

$$p_{11} > p_{22} \left(\frac{t_2}{q_1} \right)^2 + \frac{p_{22}}{q_1^2} \left| \left(\frac{s_2}{c_2^3} + \frac{s_2}{c_2} \right) \right| |\tilde{q}_2| \quad (6)$$

and either the first or the second of the following conditions are satisfied

$$p_{22} \leq p_{33} \quad (7a)$$

$$p_{22} > p_{33} \text{ and } \frac{|\omega_L|}{v_L} < \frac{1}{q_1} \quad (7b)$$

Proof. The proof of this theorem is found in Appendix I.

IV. VISION-BASED RELATIVE POSE RECONSTRUCTION

In this section we describe the novel pose reconstruction algorithm used for vision-based measurements. A standard camera is used to measure the relative state (q_1, q_2, q_3) of the lead robot. We use a specific marker to provide four detectable feature points which are used to compute the desired coordinates. Each feature point is the center of two concentric circles. The points A, B, E and F shown in Fig. 2 form a square. The (virtual) points C and D are the computed midpoints of line segments AE and BF , respectively, and correspond to the center of the fiducial, which is assumed to lie above the midpoint between the lead robots wheels.



Fig. 2. Blob analysis; detected feature points are marked as red circles

The camera output is converted to a binary image. A blob analysis algorithm returns geometric information about all detected light-colored closed segments in the image. Each blob is identified by the location of its centroid in the image plane. If two centroids are closer (using a Euclidean norm) than some threshold, they are identified as one of the feature points. This algorithm returns the image coordinates of the four points A, B, E and F . In case the algorithm does not find four pairs of blobs with close enough centroids in the current image, the coordinates from the previously sampled image are returned.

The chief advantage of this algorithm is that the measurements are computed from the present frame only. Thus, initialization is not required, and errors due to large motions are not propagated.

Once the four corners of the fiducial are extracted, it remains to obtain the coordinates q_1, q_2 and q_3 . There are three planes involved in these computations:

- P1 The horizontal ground plane of the inertial or world frame
- P2 The plane of the flat fiducial in 3D coordinates
- P3 The image plane of the camera

The normal to the fiducial and the camera optical axis are parallel to the plane P1. Since the motion of both robots is entirely in P1, the effects of pinhole projection on the height and width between the markers are decoupled, allowing us to construct the inverse of the projection without difficulty. On the plane P2, the points C and D are separated by a distance d_v . Taking $z = \bar{C}_z = \bar{D}_z$ as the depth of the fiducial in the follower frame, C and D are separated by $\frac{f d_v}{z}$ in the plane P3. This separation in P3 shows up as the difference in C_y and D_y . Hence we have

$$C_y = f \frac{\bar{C}_y}{\bar{C}_z}, \quad D_y = f \frac{\bar{D}_y}{\bar{D}_z}$$

$$D_y - C_y = f \frac{\bar{D}_y - \bar{C}_y}{\bar{C}_z}, \quad z = \frac{f d_v}{D_y - C_y}$$

The angular location and polar distance of the vertical line CD is then computed by

$$q_2 = \tan^{-1} \left(\frac{D_x}{f} \right), \quad q_1 = \frac{z}{\cos q_2}$$

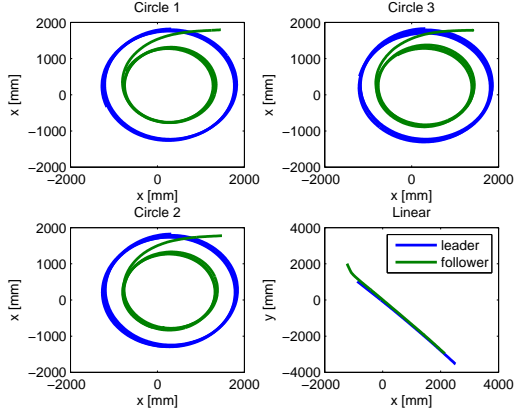


Fig. 3. The leader and follower trajectories in world coordinates

Since CD is located above the center of the leader robot, the coordinates of the leader are now known in the follower frame. Using the above methods, the points \bar{A} , \bar{E} and \bar{F} can also be reconstructed. Then, the normal vector to the plane, $P2$, in the follower robot frame is given by

$$\hat{n} = \frac{\overrightarrow{\bar{A}\bar{E}} \times \overrightarrow{\bar{F}\bar{E}}}{\|\overrightarrow{\bar{A}\bar{E}}\| \|\overrightarrow{\bar{F}\bar{E}}\|}$$

The dot product between this vector and the optical axis yields $\cos q_3$.

V. EXPERIMENTAL IMPLEMENTATION

The presented experiments utilize two iRobot Creates, one as leader and one as follower. The leader is commanded to move in a circle or a straight line. The iRobot Creates, which are controlled using QuaRC with Simulink, accept velocity commands. Hence, it is straightforward to implement our controller on them. The selected camera was a Logitech Quickcam Pro V-UA1 with a resolution of 800×600 pixels. The intrinsic and extrinsic parameters were coarsely calibrated with no obvious ill-effects. The visual servo control works well for gains that are not too large and for sufficiently slow motions of the leader in the image plane. A VICON motion capture system was used to validate the data obtained from the vision-based system [24].

Three experiments are performed where the leader moves in a circle with the same radius (See Fig. 3). A video of one

TABLE I
PARAMETERS USED IN EXPERIMENTS

	Circle 1	Circle 2	Circle 3	Linear
k_1	2e-4	2e-4	3e-4	3e-4
k_2	0.05	0.05	0.05	0.1
p_{22}	10	6	10	1
p_{33}	1	1	1	1
v_L [m/s]	0.2	0.2	0.2	0.1
ω_L [rad/s]	0.108	0.108	0.108	0
q_{1d} [m]	1	1	1	0.7
q_{2d} [rad]	0	0	0	0

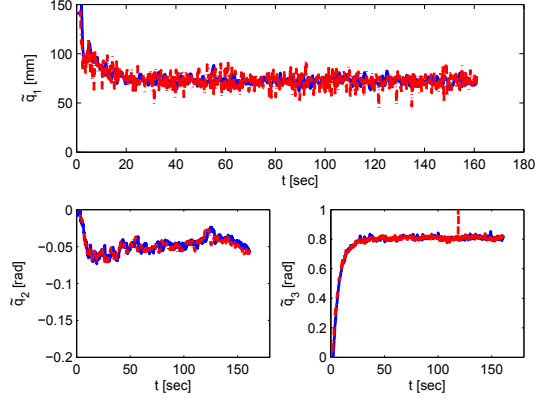


Fig. 4. [Experiment: Circle 1] The errors in relative coordinates

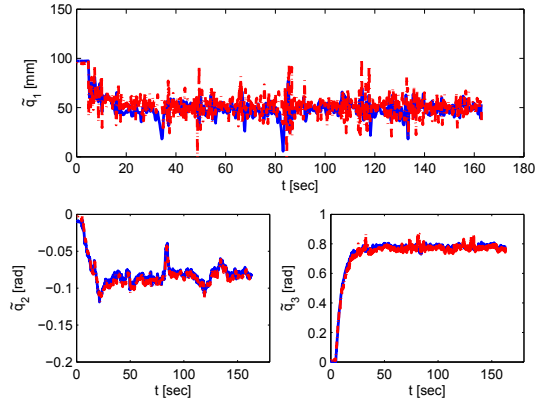


Fig. 5. [Experiment: Circle 2] The errors in relative coordinates

such experiment can be seen at <http://www.youtube.com/watch?v=4KodVTi7RcU>. The gains are varied in the experiments to demonstrate various aspects of the control (See Table I). An increase in the gain k_1 going from the first experiment ('Circle 1') to the second ('Circle 2') results in a decrease in \tilde{q}_1 , from that in Fig 4, to that in Fig. 5. In the experiment 'Circle 3', the value of p_{22} is reduced from the value in 'Circle 1'. As expected, figures 5 and 6 show that the steady state value of \tilde{q}_3 decreases while that of \tilde{q}_2 increases. We draw the attention of the reader to the good match between the VICON data (in blue in the figures) and the data from our camera-based system (in red in the figures). In addition, the marker is occasionally detected erroneously in the image, leading to spikes in the measured values of the relative coordinates. Since the feature detection is memoryless, the ill-effects of erroneous detections are minimized. Therefore, there is no need to use any estimation technique with memory, which would remove the spikes at the cost of propagating these effects through time.

The results of the experiment where the leader moves in a straight line are shown in Fig. 7, where the follower robot starts with initial relative coordinates different from their desired values. Initially, no command is given to either

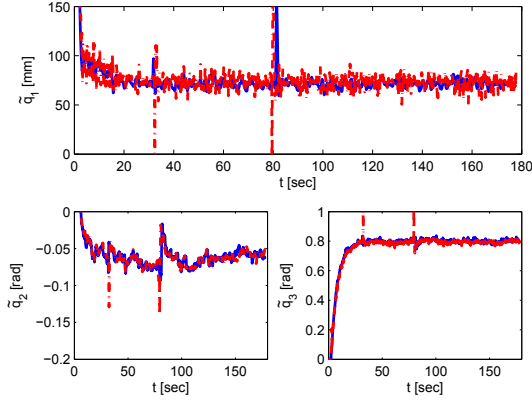


Fig. 6. [Experiment: Circle 3] The errors in relative coordinates

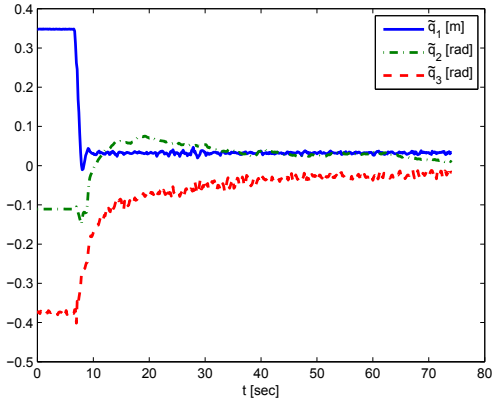


Fig. 7. [Experiment: linear motion] The errors in relative coordinates

robot. Once commands are given, the value of \tilde{q}_1 shoots quickly to a constant value. The observed steady state error in q_1 drives the robot forward. The \tilde{q}_2 and \tilde{q}_3 values decrease to zero. Due to limitations on space, the experiment could not be run until the errors in q_2 and q_3 converged to zero. However, we submit that the trend is quite clear.

VI. CONCLUSION

This paper addresses formation control of nonholonomic mobile robots with using visual servoing. A controller is presented which requires pose estimation, avoiding measurement of velocities. The pose reconstruction uses simplified homography relations and knowledge of the length between two points on a fiducial. The algorithm is memoryless, so errors in detection are not propagated in time.

The controller and vision-based-measurement pair is extremely simple to setup. It is a low-cost method of achieving uniform ultimate boundedness of the state errors. The bound can be made arbitrarily small for a straight line motion. For a general motion this is valid only for the relative distance error. The computational effort is low as the system avoids essential matrix and Euclidean homography methods to compute the pose, while, in the meantime, avoiding multiple solution problems. The only drawback is the restriction of

the movement to the plane. This restriction is valid in many applications, such as groups of robots moving at high speeds over sufficiently flat terrains.

The major restriction in the control gains stems from limited field of view of the camera. From the discussion in the last paragraph of Appendix I, one can determine the steady state value of the polar angle. The weighting between the gains p_{22} and p_{33} can then be selected such that the fiducial lies in the field of view for all time.

This work can be extended to formations of multiple robots using the same controller and vision-based measurement technique. The assignment of leader-follower pairs has been discussed in [2].

APPENDIX I PROOF OF THEOREM III.1

Consider the quadratic Lyapunov function candidate

$$V = \frac{1}{2} \tilde{q}^T P \tilde{q} \quad (8)$$

where $P = (p_{ij})$ is the matrix representation of a symmetric, positive definite transformation with the entries $p_{13} = p_{31} = p_{23} = p_{32}$ selected as zero, p_{jj} for $j = 1, 2, 3$ are positive constants and $p_{12} = p_{22} \frac{t_2}{q_1}$, where $t_2 \doteq \tan q_2$. Therefore, P is positive definite if and only if its diagonal entries are positive and

$$p_{11} - p_{22} \left(\frac{t_2}{q_1} \right)^2 > 0$$

which is guaranteed to hold by the hypotheses of the Theorem III.1. Differentiating (8) along the trajectories of \tilde{q} , and collecting the terms involving, v , ω , v_L , and ω_L ones arrives at the expression in (9).

$$\begin{aligned} \dot{V} = & (\Lambda_1 \tilde{q}_1 + \Lambda_2 \tilde{q}_1 \tilde{q}_2) v \\ & - \left(p_{22} \frac{t_2}{q_1} \tilde{q}_1 + p_{22} \tilde{q}_2 + p_{33} \tilde{q}_3 + \frac{p_{22}}{q_1 c_2^2} \tilde{q}_1 \tilde{q}_2 \right) \omega \quad (9) \\ & + (\Theta_1 \tilde{q}_1 + \Theta_2 \tilde{q}_2 + \Theta_3 \tilde{q}_1 \tilde{q}_2) v_L + p_{33} \tilde{q}_3 \omega_L \end{aligned}$$

Note that with the controller selected as in (5), the first two terms in equation (9) become negative semi-definite for all $\tilde{q} \in D$.

Selecting p_{11} such that the only nullspace of v is $\tilde{q}_1 = 0$ will ensure that $\tilde{q}_1 \rightarrow 0$ as $t \rightarrow \infty$. This clarifies the purpose of the condition (6) in Theorem III.1.

The first term in (9) can dominate the forcing terms (terms involving v_L, ω_L) with large enough k_1 if $|q_1| \geq \epsilon_1$ for all $\epsilon_1 > 0$ so that $\dot{V} < 0$ and the states move towards $|q_1| = 0$. Given $k_1 > 0$, there is an $\epsilon_1 > 0$ such that if $|q_1| < \epsilon_1$, the forcing terms in \dot{V} cannot be dominated by the first term. In this case, the second term can be used to dominate the forcing terms unless given $k_2 > 0$, $p_{22} \tilde{q}_2 + p_{33} \tilde{q}_3 < \epsilon_2$, for some ϵ_2 such that $-k_2 \epsilon_2^2$ is also very close to zero.

This discussion implies that the states tend to a neighborhood of the set $N = \{\tilde{q} \in D : \tilde{q}_1 = 0 \text{ and } p_{22} \tilde{q}_2 + p_{33} \tilde{q}_3 = 0\}$. Next, we show that if $\omega_L = 0$, then the forcing function is actually negative definite on the set N . Moreover, in the neighborhood of N , the forcing function is only positive for

very small values of \tilde{q}_2 and this positivity depends on how far the states are allowed to be from N by the individual choices of k_1 and k_2 . This implies, all states go to a neighborhood of the origin, the radius of which is determined by how large k_1 and k_2 are selected.

Since $|q_1| < \epsilon_1$, the only coefficient of v_L that can be large is $\Theta_2 \tilde{q}_2$. Apparently, Θ_2 is an odd function of q_3 with $\Theta_2 < 0$ if $q_3 < 0$. This means, $q_3 \Theta_2 > 0$ for all q_3 . On N , we have $\tilde{q}_2 = -\frac{p_{33}}{p_{22}} q_3$, so that, $\Theta_2 \tilde{q}_2 < 0$, and thus, so is \dot{V} . By the continuity of $\Theta_2 \tilde{q}_2$, there exists at least one neighborhood of N where $\Theta_2 \tilde{q}_2 < 0$. As a result, for a straight line motion of the leader, there is a neighborhood of the origin that is uniformly ultimately bounded, with the bound determined by the controller gains k_1 and k_2 .

If $\omega_L \neq 0$, the last forcing term in equation (9) can be positive. However, this positivity is overcome again by the negative definite function $\Theta_2 \tilde{q}_2$ introduced in the preceding paragraph, as follows. If either (1) $\frac{p_{33}}{p_{22}} \geq 1$, or (2) $\frac{p_{33}}{p_{22}} < 1$ and $\frac{|\omega_L|}{v_L} < \frac{1}{q_1}$ holds, then there exist $q_3 : |q_3| < \frac{\pi}{2}$ such that

$$\left| \frac{\sin q_3}{\cos q_2} \right| > q_1 \frac{|\omega_L|}{v_L} = \kappa q_1 \quad (10)$$

where $\kappa := \frac{|\omega_L|}{v_L}$ is the instantaneous radius of curvature. This clarifies the purpose of condition (7) in Theorem III.1.

As a result, the system is also stable in the presence of a nonzero rotational motion of the leader WMR with the trajectories bounded in the region defined by $N \cap \{\tilde{q} \in D : \left| \frac{\sin q_3}{\cos q_2} \right| > q_1 \frac{|\omega_L|}{v_L}\}$.

Finally, it is notable that, we can determine the fixed point of the system if the leader is undergoing a circular motion (for a straight line motion, the origin is the fixed point). For a circular motion, the radius of curvature is a constant. Assuming that the motion is restricted to N , we replace q_2 by $-\frac{p_{33}}{p_{22}} q_3 + q_{2d}$ and solve equation (10), holding with equality, for q_3 . Since $q_1 = q_{1d}$ and q_2 is a function of q_3 on N , this yields the fixed point of the system in the case of a circular motion. Given a leader trajectory, this defines the follower trajectory. If the leader is performing a more complex motion, then although there is no fixed point of the differential equations, the bounds on the states can be tightened by going through the same procedure and replacing the constant curvature by the supremum of the curvature of the complex motion.

REFERENCES

- [1] N. Leonard and E. Fiorelli, "Virtual leaders, artificial potentials and coordinated control of groups," in *Decision and Control, 2001. Proceedings of the 40th IEEE Conference on*, vol. 3, 2001, pp. 2968–2973 vol.3.
- [2] J. Desai, J. Ostrowski, and V. Kumar, "Modeling and control of formations of nonholonomic mobile robots," *Robotics and Automation, IEEE Transactions on*, vol. 17, no. 6, pp. 905–908, dec 2001.
- [3] T. Balch and R. Arkin, "Behavior-based formation control for multi-robot teams," *Robotics and Automation, IEEE Transactions on*, vol. 14, no. 6, pp. 926–939, dec 1998.
- [4] J. Lawton, R. Beard, and B. Young, "A decentralized approach to formation maneuvers," *Robotics and Automation, IEEE Transactions on*, vol. 19, no. 6, pp. 933–941, dec. 2003.
- [5] M. A. Lewis and K.-H. Tan, "High precision formation control of mobile robots using virtual structures," *Autonomous Robots*, vol. 4, pp. 387–403, 1997, 10.1023/A:1008814708459. [Online]. Available: <http://dx.doi.org/10.1023/A:1008814708459>
- [6] J. Fax and R. Murray, "Information flow and cooperative control of vehicle formations," *Automatic Control, IEEE Transactions on*, vol. 49, no. 9, pp. 1465–1476, sept. 2004.
- [7] W. Ren, "Consensus based formation control strategies for multi-vehicle systems," in *American Control Conference, 2006*, june 2006, p. 6 pp.
- [8] A. Das, R. Fierro, V. Kumar, J. Ostrowski, J. Spletzer, and C. Taylor, "A vision-based formation control framework," *Robotics and Automation, IEEE Transactions on*, vol. 18, no. 5, pp. 813–825, oct 2002.
- [9] R. Vidal, O. Shakernia, and S. Sastry, "Following the flock [formation control]," *Robotics Automation Magazine, IEEE*, vol. 11, no. 4, pp. 14–20, dec. 2004.
- [10] Y. Masutani, M. Mikawa, N. Maru, and F. Miyazaki, "Visual servoing for non-holonomic mobile robots," in *Intelligent Robots and Systems '94. Advanced Robotic Systems and the Real World, IROS '94. Proceedings of the IEEE/RSS/IGI International Conference on*, vol. 2, sep 1994, pp. 1133–1140 vol.2.
- [11] F. C. B. Espiau and P. Rives, "A new approach to visual servoing in robotics," in *Geometric Reasoning for Perception and Action*, ser. Lecture Notes in Computer Science, C. Laugier, Ed., vol. 708. Springer Berlin / Heidelberg, pp. 106–136. [Online]. Available: http://dx.doi.org/10.1007/3-540-57132-9_8
- [12] N. Gans, A. Dani, and W. Dixon, "Visual servoing to an arbitrary pose with respect to an object given a single known length," in *American Control Conference, 2008*, june 2008, pp. 1261–1267.
- [13] F. Chaumette and S. Hutchinson, "Visual servo control. i. basic approaches," *Robotics Automation Magazine, IEEE*, vol. 13, no. 4, pp. 82–90, dec. 2006.
- [14] D. F. Dementhon and L. S. Davis, "Model-based object pose in 25 lines of code," *International Journal of Computer Vision*, vol. 15, pp. 123–141, 1995, 10.1007/BF01450852. [Online]. Available: <http://dx.doi.org/10.1007/BF01450852>
- [15] L. Quan and Z. Lan, "Linear n-point camera pose determination," *Pattern Analysis and Machine Intelligence, IEEE Transactions on*, vol. 21, no. 8, pp. 774–780, aug 1999.
- [16] R. Hartley, "In defence of the 8-point algorithm," *Computer Vision, IEEE International Conference on*, vol. 0, p. 1064, 1995.
- [17] O. Faugeras and F. Lustman, "Motion and structure from motion in a piecewise planar environment," *Intl. J. Pattern Recognition and Artificial Intelligence*, vol. 3, pp. 485–508, 1998.
- [18] H. Bai, K. Chapin, J. Wason, and J. Wen, "Experimental verification of formation control with distributed cameras," in *Decision and Control, 2009 held jointly with the 2009 28th Chinese Control Conference. CDC/CCC 2009. Proceedings of the 48th IEEE Conference on*, dec. 2009, pp. 2996–3001.
- [19] Y. Igarashi, T. Hatanaka, M. Fujita, and M. Spong, "Passivity-based attitude synchronization in $se(3)$," *Control Systems Technology, IEEE Transactions on*, vol. 17, no. 5, pp. 1119–1134, sept. 2009.
- [20] G. Mariottini, F. Morbidi, D. Prattichizzo, N. Vander Valk, N. Michael, G. Pappas, and K. Daniilidis, "Vision-based localization for leader-follower formation control," *Robotics, IEEE Transactions on*, vol. 25, no. 6, pp. 1431–1438, dec. 2009.
- [21] A. Dani, N. Gans, and W. Dixon, "Position-based visual servo control of leader-follower formation using image-based relative pose and relative velocity estimation," in *American Control Conference, 2009. ACC '09*, june 2009, pp. 5271–5276.
- [22] G. Mariottini, G. Pappas, D. Prattichizzo, and K. Daniilidis, "Vision-based localization of leader-follower formations," in *Decision and Control, 2005 and 2005 European Control Conference. CDC-ECC '05. 44th IEEE Conference on*, dec. 2005, pp. 635–640.
- [23] Z. Li, Y. Ma, and T. Ren, "Formation control of multiple mobile robots systems," in *Intelligent Robotics and Applications*, ser. Lecture Notes in Computer Science, C. Xiong, H. Liu, Y. Huang, and Y. Xiong, Eds., vol. 5314. Springer Berlin / Heidelberg, pp. 75–82. [Online]. Available: http://dx.doi.org/10.1007/978-3-540-88513-9_9
- [24] Vicon Motion Systems Ltd, "<http://www.vicon.com/products/viconmx.html>."